DOT/FAA/TC-22/48

Federal Aviation Administration
William J. Hughes Technical Center
Aviation Research Division
Atlantic City International Airport
New Jersey 08405

Practical Lessons Learned from Planning, Collecting, Processing, and Analyzing Small Unmanned Aircraft System Data for Airfield Pavement Inspection

December 2022

Final Report

This document is available to the U.S. public through the National Technical Information Services (NTIS), Springfield, Virginia 22161.

This document is also available from the Federal Aviation Administration William J. Hughes Technical Center at actlibrary.tc.faa.gov.

U.S. Department of Transportation
Federal Aviation Administration

NOTICE

Technical Report Documentation Page

1. Report No.	2. Government Accession No.	3. Recipient's Catalog No.
DOT/FAA/TC-22/48	None	None

4. Title and Subtitle	5. Report Date
PRACTICAL LESSONS LEARNED FROM PLANNING, COLLECTING, PROCESSING, AND ANALYZING SMALL UNMANNED AIRCRAFT SYSTEM DATA FOR AIRFIELD PAVEMENT INSPECTION	December 2022
	6. Performing Organization Code: None

7. Author(s)	8. Performing Organization Report No.
Md Abdullah All Sourav, Halil Ceylan, Colin Brooks, David Peshkin, Sunghwan Kim, Rick Dobson, Abby Jenkins, and Chris Cook	None

9. Performing Organization Name and Address	10. Work Unit No. (TRAIS)
Department of Civil, Construction and Environmental Engineering (CCEE) College of Engineering Iowa State University 813 Bissell Road Ames, Iowa	None
	11. Contract or Grant No.: 692M15-20-T-00039

12. Sponsoring Agency Name and Address	13. Type of Report and Period Covered
U.S. Department of Transportation Federal Aviation Administration Airport Engineering Division 800 Independence Ave., SW Washington, DC 20591	Final Report
	14. Sponsoring Agency Code: AAS-110

15. Supplementary Notes

The Federal Aviation Administration Aviation Research Division Contracting Officer Representatives (CORs) were Mr. Mike DiPilato and Mr. Matthew Brynick.

16. Abstract

A small unmanned aircraft system (sUAS) or drone has proven to be a valuable tool for civil infrastructure inspection, highway inspection, unpaved road inspection, bridge inspection, construction work progress monitoring, and other applications. Additionally, several proof-of-concept studies showed that sUAS could be helpful for airfield pavement distress detection. This report documents a comprehensive study that evaluated the usefulness of sUAS-collected data in detection and rating both asphalt concrete and Portland cement concrete pavement distresses. Multiple sUASs were deployed at different altitudes to collect data from six airports in Michigan, Illinois, Iowa, and New Jersey. The collected data were then processed to create red, green, and blue (RGB) orthophotos, Digital Elevation Models (DEMs), hillshades from DEMs, and stereo-thermal orthophotos to assess what resolution and methods were best to detect and rate each type of airfield pavement distress. Based on the subsequent analysis, 1.5-mm/pix resolution for RGB orthophotos and a 6.0-mm/pix resolution for DEMs are recommended to detect and rate airfield pavement distresses. During data collection and processing, recommended standard processes were established, such as the use of high-quality ground control points (GCPs) for data acquisition, a maximum distance of 100 m between two GCPs, and a minimum three-person data collection team. Additionally, it is recommended to ensure the usability of flight-control software prior to data collection and the scheduling of sUAS deployment during low wind speed and precipitation free weather conditions. With these recommended practices in place, sUAS data can be collected effectively, safely, and efficiently. In addition, using the recommended data resolutions, most severity levels of airfield asphalt and Portland concrete cement distresses could be identified and rated.

17. Key Words	18. Distribution Statement
Small unmanned aircraft system, Airfield pavement distress, Drone in transportation, Drone in inspection, Digital Elevation Model, Orthophotos, Pavement damage detection	This document is available to the U.S. public through the National Technical Information Service (NTIS), Springfield, Virginia 22161. This document is also available from the Federal Aviation Administration William J. Hughes Technical Center at actlibrary.tc.faa.gov.

19. Security Classif. (of this report)	20. Security Classif. (of this page)	21. No. of Pages	22. Price
Unclassified	Unclassified	39	

ACKNOWLEDGEMENTS

The authors gratefully acknowledge the Federal Aviation Administration for supporting this study and would like to specifically thank the project technical points of contact, Mike DiPilato and Matthew Brynick, for their invaluable guidance, support, and direction.

Special thanks to the following airport managers for their full support during data collection:

- Grosse Ile Municipal Airport managers, Michael Duker and Janel Macnee
- Custer Airport manager, Dan Diesing
- Coles County Memorial Airport manager, Andrew Fearn
- Boone Municipal Airport manager, Dale Farnham
- Perry Municipal Airport manager, Jonathan Walter
- Cape May County Airport manager, Thomas Berry

The authors would like to express their sincere gratitude to Yongsung Koh, Robin Valle, Md Jibon, Ankita Mandelia, Vanessa Barber, Ben Hart, Julie Carter, Abby Jenkins, Kyle Potvin, Peter-Paul Dzwilewski, Trent Montgomery, Katie Gauthier, and other team members from Iowa State University, Michigan Tech Research Institute, and Applied Pavement Technology, Inc., who assisted with data collection and organization.

We also would like to express our gratitude to Adam Shover and William H. Smith, contractors from the Federal Aviation Administration, for their kind assistance with efficiency of sUAS data collection.

TABLE OF CONTENTS

LIST OF FIGURES

LIST OF TABLES

LIST OF ACRONYMS

3D	Three dimensional
AC	Asphalt concrete
ASR	Alkali-silica reaction (or reactivity)
BNW	Boone Municipal Airport
cm	Centimeter
DEM	Digital Elevation Model
DJI	Da-Jiang Innovations
FAA	Federal Aviation Administration
FLIR	Forward-looking infrared
FOG	Foot-on-ground
FOV	Field of view
GCP	Ground control point
GIS	Geographic information system
GPS	Global Positioning System
km/h	Kilometers per hour
L&T	Longitudinal and transverse
LTD	Longitudinal, transverse, and diagonal
mp	Megapixel
M2EA	DJI Mavic 2 Enterprise Advanced
mm/pix	Millimeters per pixel
MTO	Coles County Memorial Airport
ONZ	Grosse Ile Municipal Airport
PCC	Portland cement concrete
PCI	Pavement Condition Index
PMP	Pavement Management Programs
PRO	Perry City Municipal Airport
RGB	Red, green, and blue
RTK	Real-time kinetic
SfM	Structure-from-motion
sUAS	Small unmanned aircraft system
TTF	Custer Airport
VTOL	Vertical takeoff and landing
WWD	Cape May County Airport

EXECUTIVE SUMMARY

The use of small unmanned aircraft system (sUAS) in transportation fields has increased in recent times. Several proof-of-concept studies showed that sUAS could be helpful for the detection of airfield pavement distresses. Although detailed research on sUAS use in airport applications is lacking, the Federal Aviation Administration (FAA) has been testing sUAS's functionality and safety as their use becomes more prevalent. As part of this effort, this study was conducted to evaluate the performance of sUAS in detecting and rating as many airfield pavement distresses as possible and to develop guidelines and recommendations for their use in airfield pavement inspection.

In this study, different types of sUAS data were collected from different altitudes at six airports in Michigan, Illinois, Iowa, and New Jersey from December 2020 to November 2021 to determine the best methods, format, and resolution for the identification of each type of airfield pavement distress. The collected data were processed to create red, green, and blue (RGB) or "natural color" orthophotos, Digital Elevation Models (DEMs), hillshades from DEMs, and stereo-thermal orthophotos. High-resolution (less than 5 millimeters per pixel [mm/pix]) RGB orthophoto effectively identified many distresses, and lower-resolution data sets were useful for identifying a limited number of distresses. The DEMs derived using RGB optical data were mainly helpful in confirming the suspected location of the pavement distresses with elevation differences, such as faulting, shoving, depression, and medium- and high-severity crack-based distresses. Thermal data were shown to be useful for identifying certain distresses and foreign object damage as they exhibit a different thermal profile compared to intact concrete or asphalt pavement.

The recommended resolution of RGB optical orthophoto and DEM are 1.5 mm/pix and 6.0 mm/pix, respectively. During data collection and processing, recommended standard processes were established, such as the use of high-quality, ground control points (GCPs) data acquisition, a maximum distance of 100 m between GCPs, and a minimum three-person data collection team. Additionally, it was found that ensuring the useability of flight control software a week before data collection and scheduling sUAS deployment during weather conditions with no precipitation and acceptable winds predicted were also recommended. With these recommended practices in place, most severity levels of airfield asphalt and Portland concrete cement distresses could be identified and rated.

1. INTRODUCTION

The use of small unmanned/uncrewed aircraft system (sUAS), also known as drones, in the field of transportation has recently increased. This technology has proven valuable in infrastructure monitoring, crash investigation, mast light post-inspection, bridge inspection, construction work progress monitoring, and more (Banks et al., 2018; Brooks et al., 2018; Dobson et al., 2014; FHWA, 2018; Humpe, 2020; Seo et al., 2018). In addition, several proof-of-the-concept studies showed that sUASs could be helpful for the detection of airfield pavement distresses (Airsight, 2020a, 2020b; Hubbard et al., 2017; National Academies of Sciences, Engineering, 2020). However, no detailed research has been conducted so far to study the use of sUASs in this airfield pavement management and inspection. The Federal Aviation Administration (FAA) has been testing sUASs' functionality and safety as their use becomes more prevalent. As part of such an effort, this study aims to evaluate the performance of sUASs in detecting and rating as many airfield pavement distresses as possible and to develop guidelines and recommendations for their use in airfield pavement inspection. A research team consisting of members from Iowa State University, Research Institute of Michigan Technological University, and Applied Pavement Technology, Inc., visited six airports between December 2020 to November 2021 and collected data which were processed to create red, green, and blue (RGB) or "natural color" orthophotos, Digital Elevation Models (DEMs), grayscale three-dimensional (3D) terrain representations (or hillshades) from DEMs, and stereo thermal orthophotos. The processed data were analyzed for their usefulness in detecting and rating as many airfield pavement distresses as possible. Sourav, Ceylan, Brooks et al. (2022) have discussed the lessons learned from these data collection, processing, and field demonstration. It was also observed that sUAS-collected RGB data are useful to detect crack based distresses in both asphalt concrete (AC) and Portland cement concrete (PCC) pavement (Sourav, Mahedi, et al., 2022). Additionally, DEM and RGB data is adequate to detect joint deal damage, spalling, popouts, scaling, Alkali-silica reaction (ASR), and patching (Sourav, Ceylan, Kim, et al., 2022). This report presents additional lessons learned regarding selection of appropriate sUAS, types of data to collect, efficient data collection, faster data processing, and types of data to use to detect airfield pavement distresses. This report also includes a summary of the observations and additional conclusions made based on the deployment of different sUAS, as well as the use of RGB, DEM, and thermal data in airfield pavement detection and rating.

The focus was to evaluate the ability of technologies to generate a pavement condition index (PCI) or partial PCI, which can be helpful in assisting with Pavement Management Programs (PMPs). The report is organized into the following sections:

Section 2 sUAS Platforms
Section 3 Sensors
Section 4 Practical Data Collection Approach
Section 5 Data Processing and Analysis
Section 6 Useful Data Type and Resolution

2. sUAS PLATFORMS

Six sUAS platforms were deployed for data collection at Grosse Ile Municipal Airport (ONZ) in Grosse Ile, Michigan; Custer Airport (TTF) in Monroe, Michigan; Coles County Memorial Airport (MTO) in Mattoon, Illinois; Boone Municipal Airport (BNW) in Boone, Iowa; Perry City

Municipal Airport (PRO) in Perry, Iowa; and Cape May County Airport (WWD) in Cape May, New Jersey. Some platforms had integrated sensors, and others were used to carry added payloads. The sUAS platforms were different in size, weight, and capability. However, all platforms were vertical takeoff and landing (VTOL) rotorcraft, which means they have minimal launch and recovery requirements (i.e., small area capability), can hover and detect objects from a fixed position, and are able to react quickly to changing airport flight operations. The details of the sUAS platforms are provided in Table 1. Note that the flight times are an estimate of typical performance based on the deployment efforts for this and other studies and represent the sUASs flying with the chosen sensor payload under light wind conditions of less than 16 kilometers per hour (km/h). The sUAS platforms used in this study (Figure 1) could be categorized into two classes based on weight and size: (1) relatively larger and heavier sUAS platforms capable of carrying larger camera payloads, such as the Nikon D850 45.7 megapixels (mp) and Sony Rx1R-II 42.4 mp, and (2) smaller and lightweight Da-Jiang Innovations (DJI) Mavic drones with integrated sensors.

Table 1. sUAS Platforms Deployed at Different Airports

sUAS Platform	Type	Sensor	Maximum Flight Time (minutes)	Airport Deployed
Bergen Hexacopter	Six rotors, larger	Nikon D850 45.7-mp RGB optical, FLIR Vue Pro R 512x640 Stereo thermal, Tetracam Micro-MCA6	12	ONZ, TTF, MTO, BNW, PRO
UAVSI Tarot X6	Six rotors, larger	Nikon D850 45.7-mp RGB optical	14	ONZ, TTF, WWD
MicroDrones mdMapper-1000+	Four rotors, larger	Sony RX1R-II 42.4-mp RGB optical	30	
DJI Mavic 2 Pro	Four rotors, small	20-mp RGB optical	23	ONZ, TTF, MTO, BNW, PRO, WWD
DJI Mavic 2 Enterprise Advanced	Four rotors, small	48-mp RGB optical Quad Bayer and 512x640 Stereo thermal	23	
DJI Mavic 2 Enterprise Dual	Four rotors, small	12-mp RGB optical and 120x160 Stereo thermal	23	TTF

Figure 1. Tarot X6 with Nikon D850, mdMapper-1000+, Mavic 2 Pro, Nikon D850 Camera, Mavic 2 Enterprise Advanced, Bergen Hexacopter with Nikon D850 (clockwise, from top left)

2.1 SMALL AND AGILE PLATFORMS WITH INTEGRATED SENSORS

Three small sUASs were deployed in the data collection sites, all of which included integrated sensors: DJI Mavic 2 Pro, DJI Mavic 2 Enterprise Advanced (M2EA), and DJI Mavic 2 Enterprise Dual. All three sUAS platforms weigh about 1,100 gm each. They have a maximum flight time of 31 minutes, as reported by the manufacturer, with about 23 minutes in practical use during this study, including a safety margin of about 20 to 30 percent battery life by the time the flights were completed. These small sUAS platforms showed better agility and maneuverability compared to the larger platforms. They can perform better than the larger sUAS platforms in adverse weather conditions; for example, the M2EA and Mavic 2 Pro were deployed safely and successfully at TTF with up to 40 km/h wind gusts. Multiple successful flights were conducted at several airports with these platforms despite wind gusts of more than 25 km/h. In addition, DJI provides and maintains flight assistant software for these sUASs, which is reliable and easy to use (DJI Go 4 for the Mavic 2 Pro, DJI Pilot for the M2EA). In addition, the DJI smart controller that is included with the M2EA facilitates easy mission planning, data collection, and collection monitoring, with no need for an additional smartphone or tablet computer; however, external internet access must be provided to access the basemaps (such as existing aerial photos) when in the field. The bright screen and high battery capacity of the controller made it suitable for fast and quick data collection. DJI and third-party flight assistant applications, such as DroneDeploy® and Pix4D® Capture, support continuous data collection with low-battery-swap downtime (2–3 minutes). For an example of efficient data collection, in May 2021, the research team collected data over 1,523 m x 30 m (4.6 hectares) on Runway 3/21 at TTF within 3 hours and 20 minutes, where the software showed that the mission time was slightly over 2 hours.

Based on use during this study, these small sUAS platforms have two disadvantages: (1) users cannot mount any significant payloads (such as additional sensors, e.g., optical or thermal cameras), and (2) automatic missions are not supported for very low altitudes on the mission

planning software provided by the manufacturer. For example, the DJI flight assistant mobile applications for the sUASs used in this study only allow collecting RGB optical data at 15 m or higher and stereo thermal data at 24 m or higher.

2.2 HEAVIER PLATFORM WITH AN ADDITIONAL PAYLOAD CAPACITY

Three relatively large sUAS platforms, weighing between 6 kg and 10 kg with batteries on board, were also deployed. These sUAS platforms were mainly used for high-resolution sample unit data collections because of their ability to carry heavier, high-resolution cameras. The newer Tarot X6® platform from UAV Systems International (Figure 1, top left) was used to complete a significant data collection at WWD in August 2021, ONZ in November 2021, and TTF in November 2021. The platforms are versatile, and different sensors can be mounted based on the research need. The RGB optical cameras mounted on these platforms are full-frame and high-resolution devices capable of capturing superior data compared to the smaller platforms' integrated, lower-resolution RGB optical sensors. Thus, these cameras mounted on larger platforms are recommended for higher resolution data collection requiring 2-mm/pix or better resolution RGB imagery with 6-mm/pix or better resolution DEM results for identification and rating of as many pavement distresses as possible.

3. SENSORS

Two types of sensors were deployed to study their usefulness in detecting and rating airfield pavement distresses: RGB optical for creating orthophotos and DEMs, and longwave thermal infrared collected in stereo data collection mode to create merged thermal image outputs. In addition, a multispectral sensor able to collect visible and near-infrared light wavelengths was deployed for an initial short demonstration, which was later discontinued. RGB optical sensors were deployed multiple times at different altitudes to obtain different resolutions and to determine the best resolution to detect and rate the pavement distresses or damage present at the parts of airports studied. Table 1 shows the sensors, altitudes, and output resolutions of all sensors used in this study.

RGB optical sensors were used extensively in this study. The Nikon D840 45.7-mp and Sony RX1R-II 42.4-mp RGB optical sensors are high-resolution, full-frame sensors mounted on larger sUAS platforms that can carry these heavier payloads. Deploying such sensors requires a detailed understanding of the camera's settings, which need to be adjusted based on the light (sunlight and cloud) conditions. The integrated sUAS sensors onboard the three DJI platforms were easy to use but provided relatively fewer visual details of airfield pavement than the full-frame sensors due to the higher resolution of the full-frame cameras. For integrated sUAS sensors, this study tested the sensors of the three DJI Mavic platforms that were deployed: 12-mp RGB optical sensor of Mavic 2 Enterprise Dual, 20-mp RGB optical sensor of Mavic 2 Pro, and 48-mp Quad Bayer RGB optical sensor of M2EA.

Two thermal and one multispectral sensors were also used for this study. Initially, a forward-looking infrared (FLIR) Vue Pro R was mounted on a Bergen Hexacopter and deployed at ONZ in December 2020. The sensor does not record Global Positioning System (GPS) information along with the thermal image but has an established workflow for processing the results into usable formats, such as JPEG files with per-pixel temperature values. M2EA's thermal sensor has the

same resolution as the FLIR Vue Pro R, and the research team extensively used this newly acquired unit throughout this study—mainly because of its GPS data collection capabilities that provide location-tagged thermal images. However, the M2EA was only released in March 2021, and the processing software is not yet mature for its thermal data outputs. A well-established workflow to obtain per-pixel temperature values from the M2EA thermal sensor is being developed by the M2EA user community, as DJI's available software tool for processing M2EA does not yet yield data usable for merging geospatial data with actual temperature values. However, the M2EA data area is easily usable for analyzing relative temperature differences in airfield pavement. Despite these current limitations, it was still possible to use the M2EA data to address the utility of thermal cameras to help identify and rate pavement distresses.

The primary lessons learned from the deployment of the selected sensors include:

- Full-frame RGB camera sensors usually provide better visual details in output products with the 42.4-mp and 45.7-mp systems used in this study, but these sensors are not directly integrated with platforms. Additional knowledge and effort are required to use them for data collection.

- The ISO, which reflects the camera sensitivity to light, aperture, and shutter speed, needs to be adjusted on the non-integrated RGB full-frame cameras to capture the best quality images under different light conditions, flight altitudes, and flight speeds. These options dictate how much light the camera will allow to come through the lens. Additional equipment and processing steps are required to capture position information and geotag the collected imagery.

- Quad Bayer camera sensors do not provide the same visual details as regular sensors with similar resolution. The 20-mp integrated RGB sensor of the Mavic 2 Pro provided better details when compared with the 48-mp Quad Bayer RGB camera of the M2EA. This 48-mp camera is actually a 12-mp camera that does additional processing to improve image resolution (GSMArena, 2019).

- It is challenging to create a thermal orthomosaic image from a non-geotagged image. The field of view (FOV) of the thermal sensor is narrow, and the presence of a lower number of pixels poses extra difficulty in orthophoto generation. The narrow FOV also drastically increases the required image overlap and, therefore, the total flight time required to create a high-resolution thermal orthomosaic.

- The Tetracam Micro-MCA6, the multispectral sensor deployed at TTF, did not provide additional distress detection and analysis values in the limited testing. Thus, the multispectral data collection was not pursued further for this study but might warrant a more detailed study over more areas.

4. PRACTICAL DATA COLLECTION APPROACH

4.1 MINIMUM CREW REQUIREMENT

For most of the sUAS data collection, four or more research team members were on site. In a feasibility study to determine the minimum crew size required to collect sUAS data successfully from an airport, it was determined that a three-member sUAS crew could successfully collect sUAS data at an airport with low air traffic, without interrupting the general flow. The recommended three-person team should consist of one remote pilot in command, one visual observer, and one person responsible for managing data collection logistics. Additional activities can include charging the sUAS batteries, taking location-tagged field photos, taking some measurements of distresses that can be compared to the sUAS imaging results such as the height of shoving or swelling, and placing and removing ground control points (GCPs). It is also helpful for the crew to include at least one additional sUAS pilot with an additional dedicated observer, if possible, to enable simultaneous and fast data collection for at least two different airport locations. More paired pilot-observer teams could be deployed to quickly complete data collection at multiple locations if resources allow. Each crew needs to have a dedicated portable aviation radio for efficient and safe operations.

4.2 NUMBER OF GROUND CONTROL POINTS AND THEIR OPTIMAL LOCATIONS

The number and location of GCPs are important to meet data collection and processing needs for detection and rating of distresses by helping to create accurate orthophotos and DEMs. The presence of six or fewer GCPs on a long and narrow runway or taxiway can cause distortion of the orthophoto shape with unexpected spatial deviation. This phenomenon was observed in the TTF data collection in March 2021 and in the BNW data collection in June 2021. The number of GCPs to put on a data collection site depends on the site's shape, size, and the positional accuracy desired/needed from the sUAS data. In the later part of this study, the research team attempted to place GCPs on the four corners of the target areas first, followed by placing two GCPs on both sides of the runway or taxiway with an interval of around 100 m (Figure 2). For the approximately 1,200-m length (by 45 m wide) area of the WWD 10/28 runway, 30 GCPs were used to derive the sub-2-mm/pix RGB orthophoto and 6-mm/pix or better DEM high-resolution outputs. Priorities should be given to GCP placement close to the sample units of greatest interest. The research team also demonstrated that Propeller AeroPoints™ (Propeller, Surrey Hills, Australia) with built-in, location-recording technology (global navigation satellite systems or GNSS, referred to in the United States as GPS) can be used effectively numerous times due to their portability and capability of collecting high-resolution, better than 5-centimeter (cm) accuracy, position data within 45 minutes.

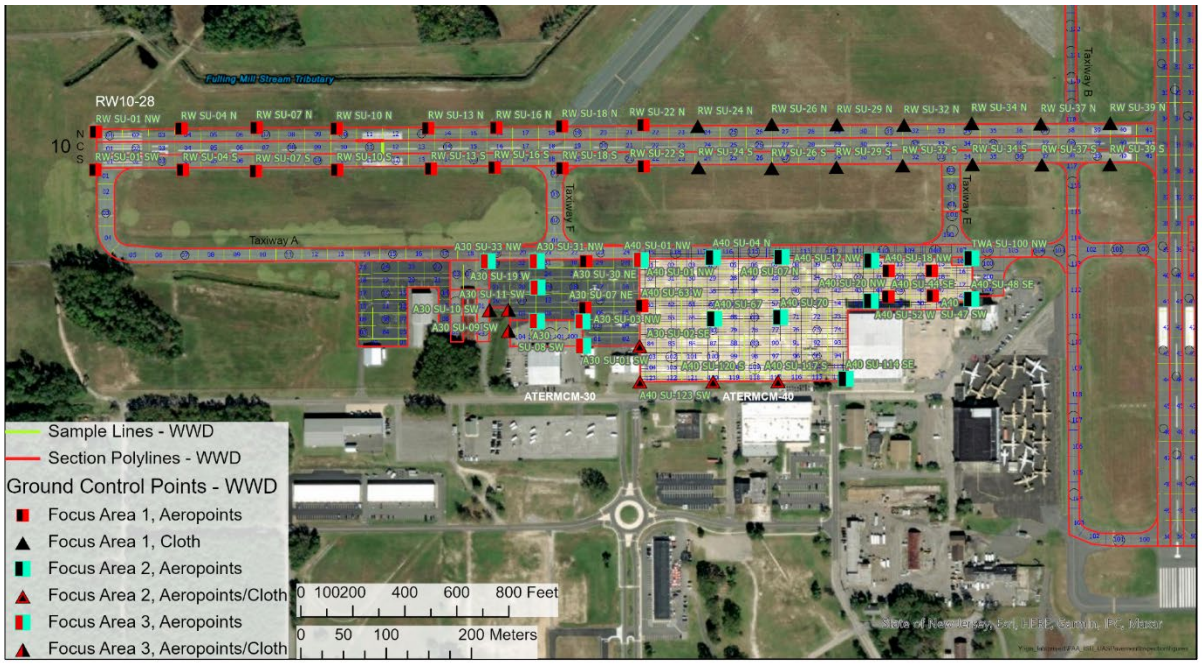

Figure 2. Ground Control Targets Locations Planned and Used at WWD

4.3 IMPACT OF WEATHER ON DATA COLLECTION

sUAS data collection generally requires favorable weather for efficient data collection, with no precipitation and reasonably low wind speeds. It is recommended to closely observe weather forecasts starting 10 days ahead of the data collection. A final call on weather conditions should be made 2 days before data collection, but this decision should be reviewed on the day of data collection. Most sUASs cannot collect usable imagery during precipitation, such as rain and snowfall, because it can affect the operations (most drones are not waterproof), and can affect the collected imagery, especially when moisture on camera lenses makes images unusable for analysis. In addition, wind speed and wind gusts must be considered before data collection. The smaller sUASs flown in this research can operate effectively at wind speeds up to 40 km/h, while the larger sUASs can successfully collect data up to 24 km/h. The platforms used in this study should not be flown for safety and imagery quality reasons at more than mentioned windspeed. It is advisable to proceed with the data collection based on the capabilities of the sUAS platforms and wind speed.

Reasonable illumination by daylight is required to collect quality sUAS imagery (nighttime artificial illumination to potentially make overnight RGB imaging possible was not within the scope of this study). Thus, the period of possible data collection in a day depends on the time of the year and the site's geographical location. The research team started collecting data as early as 8:30 AM and continued until 7:00 PM in the summer (August 2021) at WWD in New Jersey. However, in the fall, the period of available daylight shortens significantly. A field data collection in mid-November at ONZ in Michigan showed that the data collection had to start after 10:30 AM and conclude before 3:30 PM so that sufficient light for data collection was available. It is possible to collect data during both cloudy and sunny conditions, with both typically able to provide sufficient illumination. Partly cloudy conditions are possible, too. However, rapid changes in

sunny vs cloudy conditions during an sUAS flight can make the photogrammetric data results more inconsistent. Some areas show darker or brighter than others in the merged orthophoto RGB output. Distress detection is still possible with these "changing light condition" orthophoto outputs but could require more careful interpretation to understand impacts on how distresses appear. Thus, it is advisable to plan accordingly to get adequate light for RGB optical sensors.

4.4 sUAS PLATFORM SOFTWARE UPDATE AND ISSUES

The sUAS platforms are often complex technology with many hardware and software components that need to operate properly for safe, efficient, and high-quality data collections. When one or more components do not operate properly, challenges in deployment or operation can occur. For example, the research team attempted deployment of the mdMapper1000+ with Sony RX1R-II 42.4-mp optical RGB camera system at airports in Iowa; however, the system did not take off due to technical difficulties related to a recent software update that was supposed to address existing known issues. Instead, the update created new complications. Similarly, at WWD, the same unit, operating at sufficiently low wind conditions, did not collect the intended data due to an unexpected software bug in the flight control application. Thus, updating the flight controller software and sUAS platform firmware a week or more prior to data collection and avoiding any setup changes is recommended. The research team also found that the mdMapper system was more sensitive to wind conditions than the other large sUAS platforms (Bergen, Tarot X6). Its use was restricted when winds were below 16 km/h. For any platform, conducting a few pretest flights is recommended, which would be helpful to identify such issues in the weeks and days ahead of data collection to ensure that imagery will be collected as expected.

A reliability issue was observed with third-party applications (herein referred to as apps) used to control sUASs, such as the DJI Mavic 2 Pro. Software updates to flight control apps sometimes meant that software that worked for data collection one week might not work the following week. It is strongly recommended to verify that all intended flight control applications work the day before flights occur and to avoid changing any settings until after data collections are complete.

One difficulty encountered using sUAS platforms at airports was the requirement of "unlocking geozones" (or geofences) for drone flights prior to taking off at airports while using flight apps like DJI Go 4®, DJI Pilot®, and DroneDeploy®. The requirement is understandable in light of the considerable safety and security it provides for airports, but it does complicate sUAS-based data collection. Long-term geozone restrictions, such as at towered airports, are simpler to address ahead of time. However, in two untowered airports, the research team experienced temporary geozone restrictions that were difficult to unlock and delayed the data collection. While the process has become slightly more streamlined (e.g., using the Aloft® app and linking flight permissions granted to a licensed airman from Aloft® to a DJI account), this process has evolved rapidly over the past year, often with major changes occurring on a week-to-week basis. This can greatly complicate collecting data at airports, especially at locations that might not have a good cellular wireless signal to unlock a geozone once at an airport. sUAS pilots should ensure that any necessary flight permissions are obtained one or more weeks ahead of time and linked to necessary accounts. These accounts and pilots must be linked to sUAS/apps planned to be used in the field on the day of the data collection.

5. DATA PROCESSING AND ANALYSIS

5.1 DATA PROCESSING FRAMEWORK

RGB optical data were collected from all six airports visited in this study. Each photogrammetric stereo overlapping image dataset was imported separately into Agisoft Metashape® for processing (Agisoft LLC, St. Petersburg, Russia). The research team has worked extensively with this software for at least 10 years and knows its capabilities in-depth. Relative to other processing software, Agisoft Metashape®'s tunable processing steps provide more control for the image analyst. The team has also worked with Pix4D® software on occasion for other applications, including processing thermal imagery.

The positional accuracy of the sUAS imagery outputs was improved beyond what can be provided by any onboard GPS using the GCP's location recorded with the AeroPoints™ and Trimble® GeoExplorer® 6000 (Trimble Inc., Sunnyvale, California, U.S.) GPS units. The AeroPoints™ have approximately 3-cm to 5-cm x,y,z accuracy but can be better; at least 45 minutes of data collection on the ground is recommended to achieve this accuracy. The GeoExplorer® 6000 has approximately 10-cm x,y,z accuracy within 5 minutes of data collection. More expensive and modern GPS units than the GeoExplorer® 6000, ideal for achieving survey-grade accuracy in similar rugged field conditions, can achieve approximately 1-cm x,y,z accuracy with as little as 1 minute of data collection.

The images were processed using one or more high-end desktop workstations to create RGB optical orthophotos, DEMs, hillshades, and stereo thermal orthophotos. The DEM is a raster image, with each pixel representing the elevation, and the DEM was generated based on the dense cloud created using Agisoft Metashape® software as part of the RGB orthophoto production process. The final resolution of the DEM depended on the resolution of the image captured by the optical RGB sensor. Each DEM was imported to ArcGIS Pro® (ESRI, West Redlands, CA, USA) to produce a "hillshade DEM" for easier visualization and interpretation of elevation models. As described by ESRI, a hillshade is derived from the DEM and "produces a grayscale 3D representation of the terrain surface, with the sun's relative position taken into account for shading the image" (ESRI, 2021). The study team has previously found that it makes DEM data much easier to interpret, especially for visually identifying areas of greater elevation change in a data collection area. Draping a partially transparent hillshade over the DEM it was derived from was particularly helpful in identifying elevation change areas.

5.2 TIME REQUIRED FOR DATA PROCESSING AND ANALYSIS

The data-processing time for a complete data collection varies based on the resolution of the data, the number of photos in the data set, and the required resolution of the output. An image captured by a Nikon D850 45.7-mp camera contains many more pixels than another image captured by a 12-mp camera; thus, they are expected to have a longer processing time. The number of images dictates the processing time required for images with the same resolution. For example, a dataset with 2,938 images required 18 hours and 48 minutes to process, whereas 1,267 images took 7 hours and 40 minutes on a computer equipped with Intel® Xeon® W-2265 Processor (19.25 Megabyte Cache, 3.50 Gigahertz) with 12 cores and 24 threads, 128-Megabyte DDR4 ECC RAM, and NVIDIA QUADRO RTX 5000 16 Gigabyte graphic card with 3,072 CUDA Cores. The export

times for these two datasets are also different. It is also worth noting that the configuration of the workstation computer contributes to the data processing time. It is safe to assume that 2,000 to 3,000 images, each with 45.7-mp resolution, would take at least 24 hours if every step was completed as intended in the workstation mentioned above. However, the research team experience showed that some processes might need to be redone, so a 2-day time frame was estimated to be the shortest achievable processing period for such a large study on one computer, which can be typical for an airport sUAS data collection. Agisoft Metashape® allows users to use multiple computers simultaneously on a distributive network and reduce the processing time significantly, which the research team was able to benefit from in this study.

The ability to use sUAS data for airfield pavement distress identification depends on the density and types of distresses present on the sample unit. For example, several Portland cement concrete (PCC) sample units at BNW had only a handful of longitudinal, transverse, and diagonal (LTD) cracks and joint seal damage. It required an average of 5 to 10 minutes to observe and note the individual distresses visually. On the other hand, the relatively large sample units of WWD PCC sections with patching, ASR, spalling, and LTD cracks took around 40 minutes to 1 hour to visualize and record the distresses. Due to the high density of longitudinal and transverse (L&T) cracks at WWD, each AC sample unit took about 45 minutes to 1 hour to record. AC sample units of TTF required around 25 minutes as the density of cracks was considerably lower. In addition, such analysis also depends on the experience of the image analysts. For example, ONZ data that were analyzed at the beginning of this study required around 35 minutes for each sample unit. A similar analysis by the same image analyst required 20 to 25 minutes at the end of the study once the analyst was familiar with the analysis and the site.

5.3 OVERLAY OF PCI SURVEY DATA WITH sUAS DATA

The existing method of PCI surveys can and do produce geospatial data that show the locations of distresses and airport features, such as sample unit boundaries, concrete slab boundaries, and named locations of runways/taxiways/connectors. New distress data can be recorded in tablets that enable the inspector to record the location, type, and severity of distress data, with existing data such as sample unit locations displayed in the background. However, it has not previously been critical that these types of geospatial data have very high, sub-meter, absolute positional accuracy. The same has generally been true for remote-sensing products created for airports, such as aerial photography from manned aircraft or orthophotos created from sUAS-enabled photogrammetry. If these products did not "line up" with an accuracy of better than a meter, then this had little impact on rating airfield pavement condition.

However, it is important that geospatial data "line up" relatively accurately to make data easier to compare between different data creators and over time. For example, Figure 3 shows three different views of "foot-on-ground" (FOG) (manual) surveys completed for ONZ. On the left are the inspection data as shared, without any imagery background. This is a view that an inspector would see while recording new PCI data. The middle image is a view of those data when overlaid on an orthoimage created from sUAS collected imagery with an approximately 10-cm positional accuracy. The manual inspection geospatial data range from 3.1 m to 3.8 m off the location of the sUAS imagery. The right image shows the manual inspection data once they have gone through a spatial adjustment process to align them with the sUAS imagery that has better positional accuracy. These data are significantly easier to interpret and compare between different sources of imagery.

If future imagery is collected with 10-cm or better positional accuracy, this will also line up well with historical and future manual or automated inspection data.

Figure 3. Manual Distress Survey Result (left); Manual Survey Results Overlaid on an RGB Data with Approximately 10-cm Position Accuracy (middle); and Well-aligned Manual Survey Results (right)

A similar issue occurs with sUAS imagery. Depending on the quality of GPS onboard the sUAS, the image-processing methods, the use of real-time kinematic (RTK) GPS, and the use of GPS-enabled ground control targets, the absolute positional accuracy of the output products, such as orthophotos, can vary widely. Figure 4 illustrates this with an example shared by the third-party company that collected data at WWD in May 2021. One image is the 2-mm product (Figure 4, left), and the other is the 3-mm product (Figure 4, right). Their detected distress layer is shown on both—it lines up precisely with the 3-mm orthophoto output, but not the 2-mm orthophoto made by the same company. The 2-mm third-party orthophoto is shifted about 1.8 m west of the 2-mm product, most likely because the third party did not use GCPs when collecting imagery via sUAS at their airport surveys. This can make it more difficult to know which specific distress is being mapped in each case, and also means that imagery collected by other parties or in the future cannot be expected to align well. Figure 5 shows what should be expected—that manually collected distress data and future automatically detected distress data will align well (within 0.5 m or better) with orthophotos output as accurately positioned data that use 10-cm or better ground control or Real Time Kinematic/Post-Processing Kinematic technology. The manually collected FOG distress data did have to be spatially adjusted, but, in the future, the sUAS-derived orthophoto can be put in the background for field inspection tools so that recorded distress will align with sUAS outputs from the start.

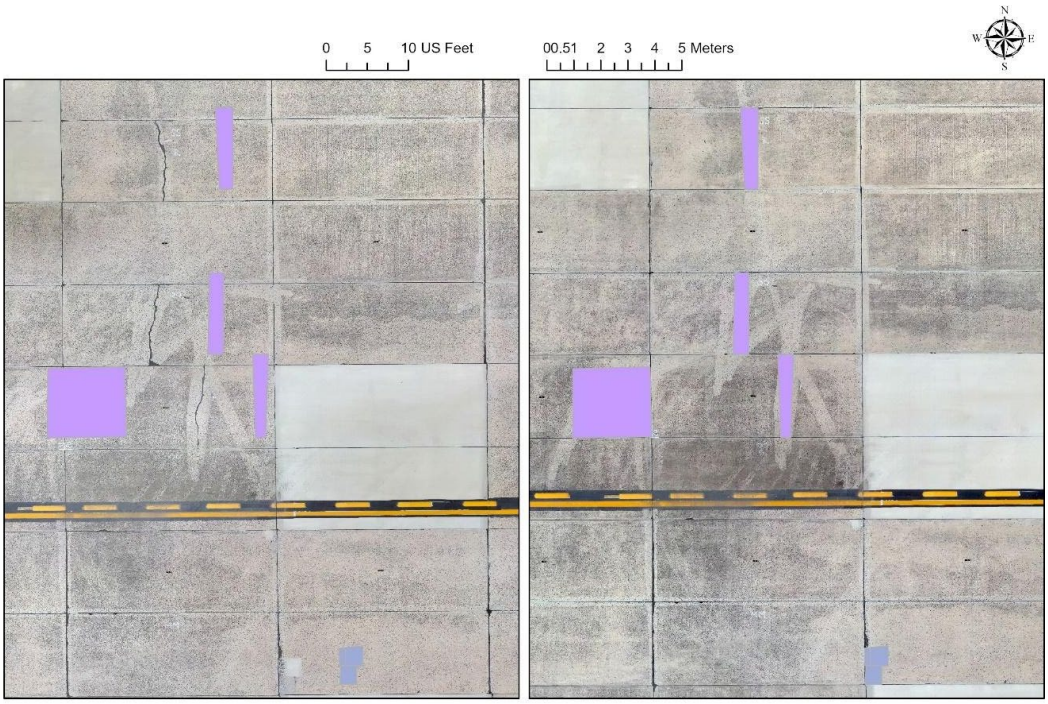

Figure 4. Third-party 2-mm/pix RGB Orthophotos Created Without GCPs (left) Located 1.8 m Away from a 3-mm/pix RGB Orthophoto (right)
(The purple polygons are created based on 3-mm/pix RGB data.)

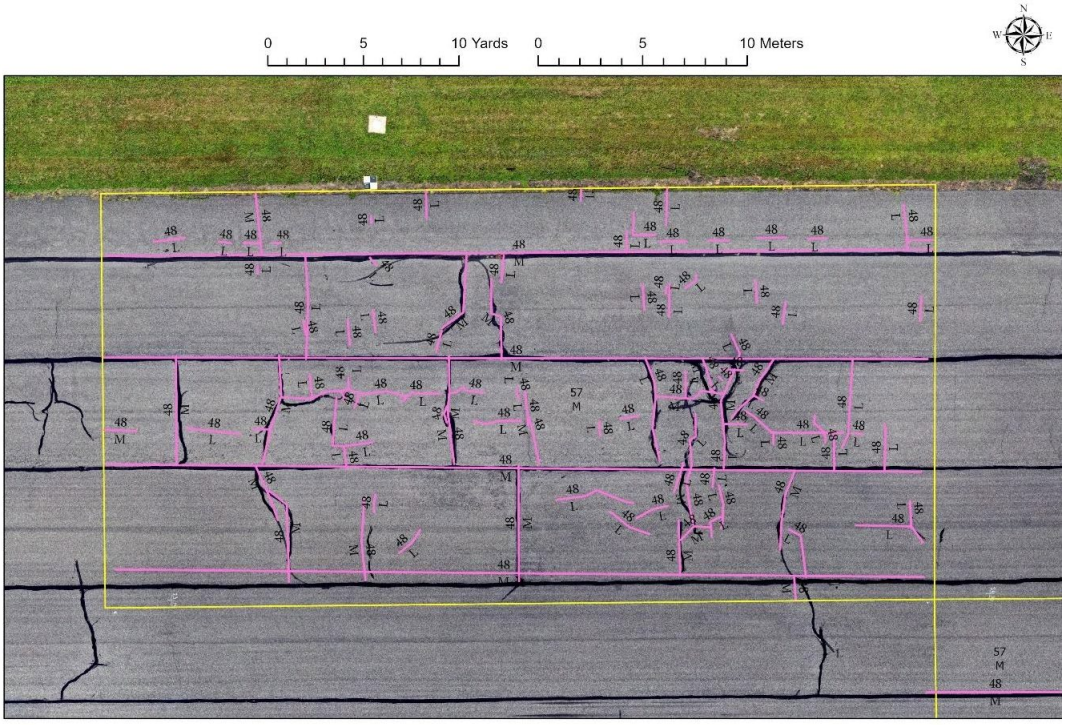

Figure 5. An Example of Recommended sUAS-assisted PCI Inspections and Geospatial Layers

Creating sUAS outputs with high positional accuracy and ensuring that PCI inspection data align well with this takes significant time, especially for spatially adjusting existing inspection geographic information system (GIS) data. However, the effort is worthwhile to ensure that future inspection data and sUAS outputs all align closely. On a practical basis, it is recommended that sUAS imagery outputs (plus DEMs and hillshades) should have at least 0.5-m absolute positional accuracy to have moderate positional accuracy, with a preference for 20 cm or better for high positional accuracy, and 10 cm or better if possible. This can be accomplished using ground control targets, such as GPS-enabled ones like the Propeller AeroPoints™, or traditional cloth or plastic targets whose locations are recorded with a 10-cm accuracy or better GPS unit. If RTK positioning can provide this accuracy with few or no GCPs, then this would be acceptable as well, but this has not been tested directly yet.

As few as 10 GCPs can work for some single-runway or single-taxiway data collections. At WWD, 60 different locations (some locations collected more than once over multiple days) were used to ensure high positional accuracy for each geospatial output. If a dedicated person collects these GCP positioning data, then this can be done while other crews focus on sUAS data collection. With a dedicated person, this can be accomplished in 2 hours or less at a two-runway untowered airport such as WWD. The amount of time will depend on the type of GPS unit used, if more than one unit is available, or if multiple GPS-enabled GCPs such as AeroPoints™ are available and can be left to collect data while other survey activities take place. One option for surveyors is to use temporary paint markings on the ground and collect GPS data (using AeroPoints™ or other GPS-enabled GCP units) over the course of the data collection. This avoids any potential issues of moving AeroPoints™ or GPS units during drone surveying, especially if multiple days are required to complete surveys. Until RTK technology is evaluated further, it is recommended to use GCPs for all sUAS airport surveys.

6. USEFUL DATA TYPE AND RESOLUTION

The demonstration of a multispectral imaging system was limited to one data collection at one airport (TTF), and the resulting images did not provide any useful details beyond the other two sensors. Additional testing could reveal further value in multispectral and potentially hyperspectral, sUAS-collected data products. However, this section only focuses on the value of the RGB optical and thermal sensor data that were explored in more detail.

6.1 RED, GREEN, AND BLUE OPTICAL DATA

RGB optical orthophotos with resolutions ranging from 0.8 mm/pix to 21 mm/pix were viewed using ArcGIS Pro to determine their usefulness in airfield pavement distress detection and rating. ASTM D5340–20 lists 16 PCC pavement distresses, and 14 were available in this study's sUAS data collection sites; blowup and pumping were not available (ASTM International, 2020). The analysis showed that the RGB optical orthophotos of 3.3-mm/pix or better resolution were sufficient to detect 13 out of 14 PCC pavement distresses, with one or more severity level(s) observed in this study. Faulting could not be detected in the surveyed locations. Visualization of different distresses with low (L), medium (M), and high (H) severity are shown in Figures 6 to 10. Eight AC pavement distresses occurred at TTF and MTO out of the 17 distresses listed by ASTM D5340-20. The analysis identified block cracking, alligator cracking, patching, and L&T cracks with RGB orthophotos; some examples are illustrated in Figures 11 and 12.

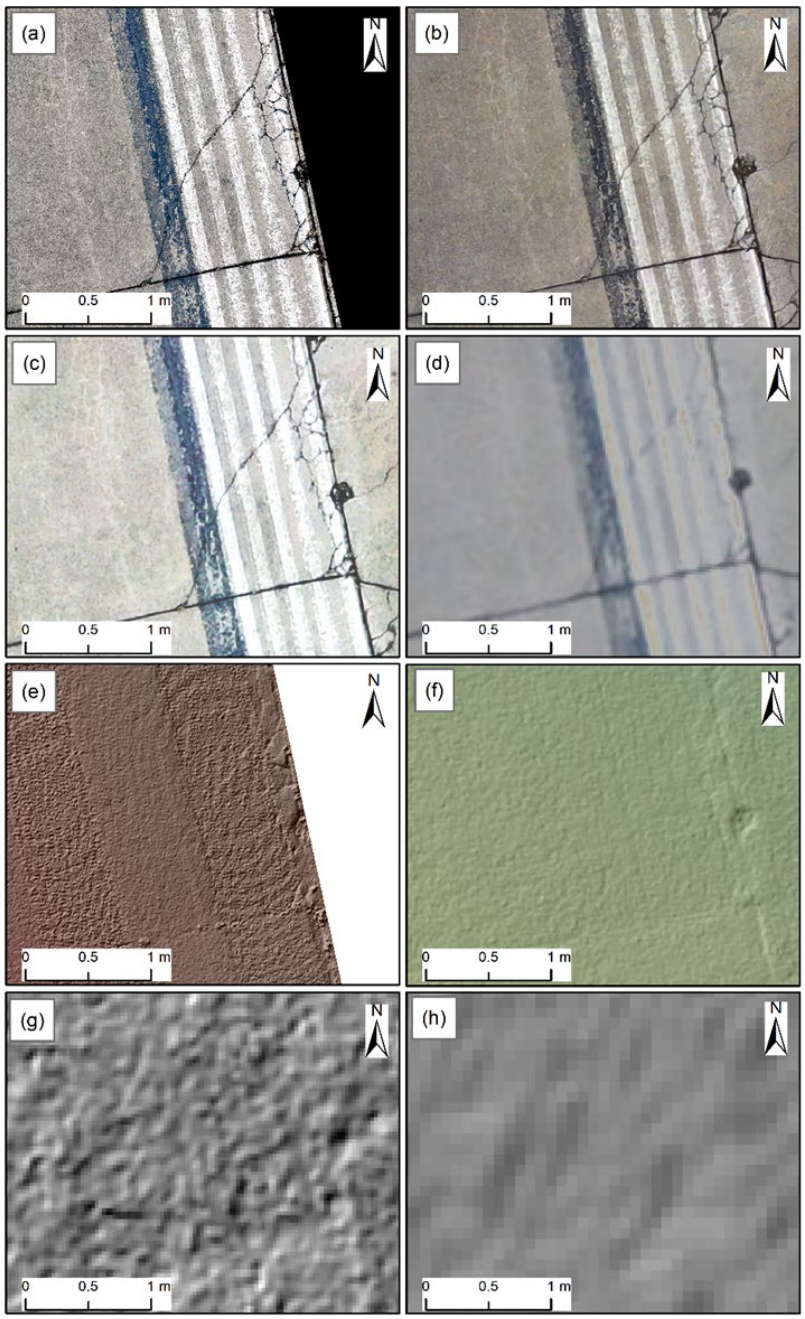

Figure 6. Corner Break (H) in (a) 0.8-mm/pix Orthophoto, (b) 2.5-mm/pix Orthophoto, (c) 7.3-mm/pix Orthophoto, (d) 21-mm/pix Orthophoto, (e) 3-mm/pix DEM, (f) 10-mm/pix DEM, (g) 29.1-mm/pix DEM, and (h) 84-mm/pix Hillshaded DEM Derived from 21-mm/pix Orthophoto

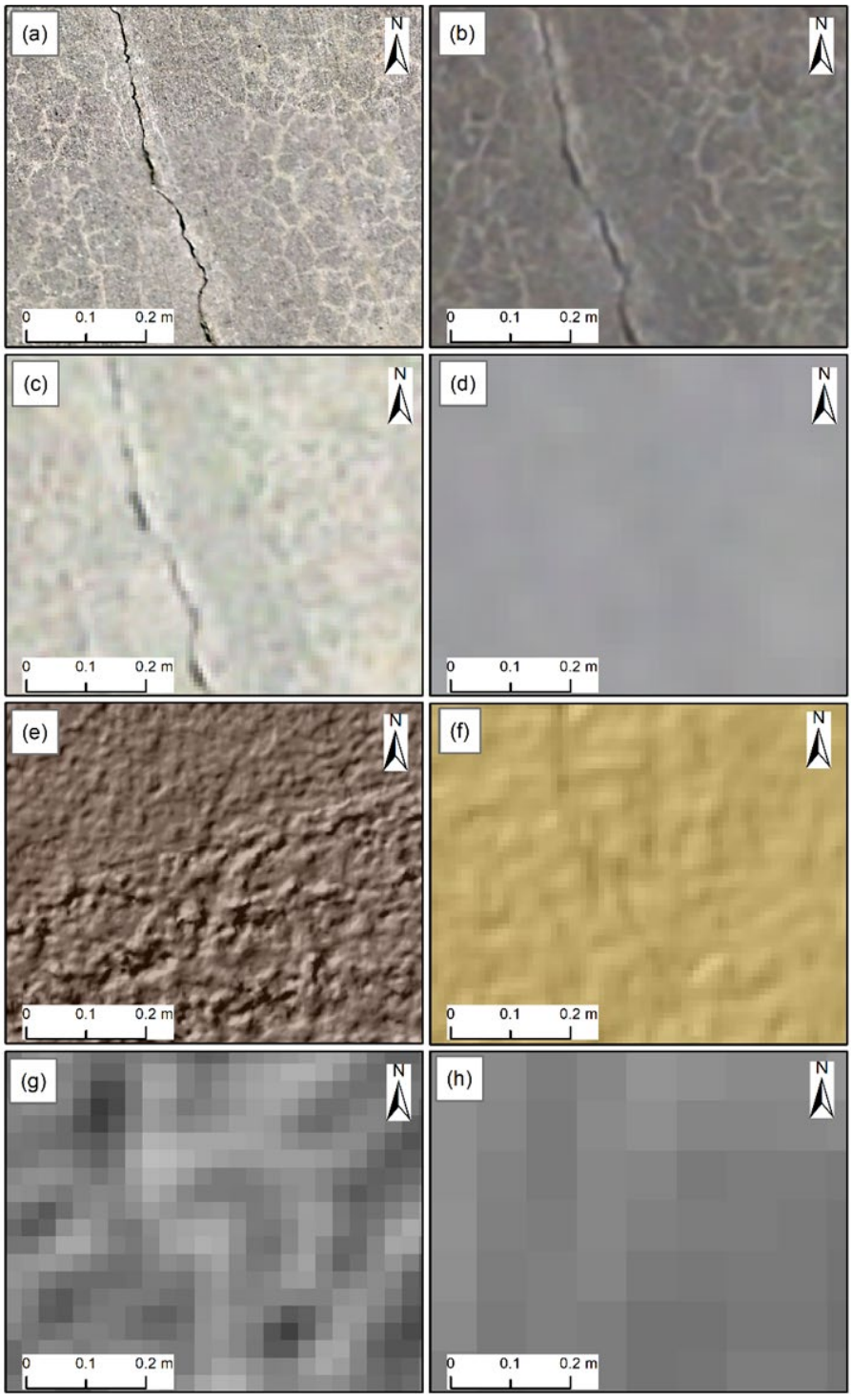

Figure 7. Longitudinal and Transverse Cracking (L) in (a) 0.8-mm/pix Orthophoto, (b) 2.5-mm/pix Orthophoto, (c) 7.3-mm/pix Orthophoto, (d) 21-mm/pix Orthophoto, (e) 3-mm/pix DEM, (f) 10-mm/pix DEM, (g) 29.1-mm/pix DEM, and (h) 84-mm/pix DEM

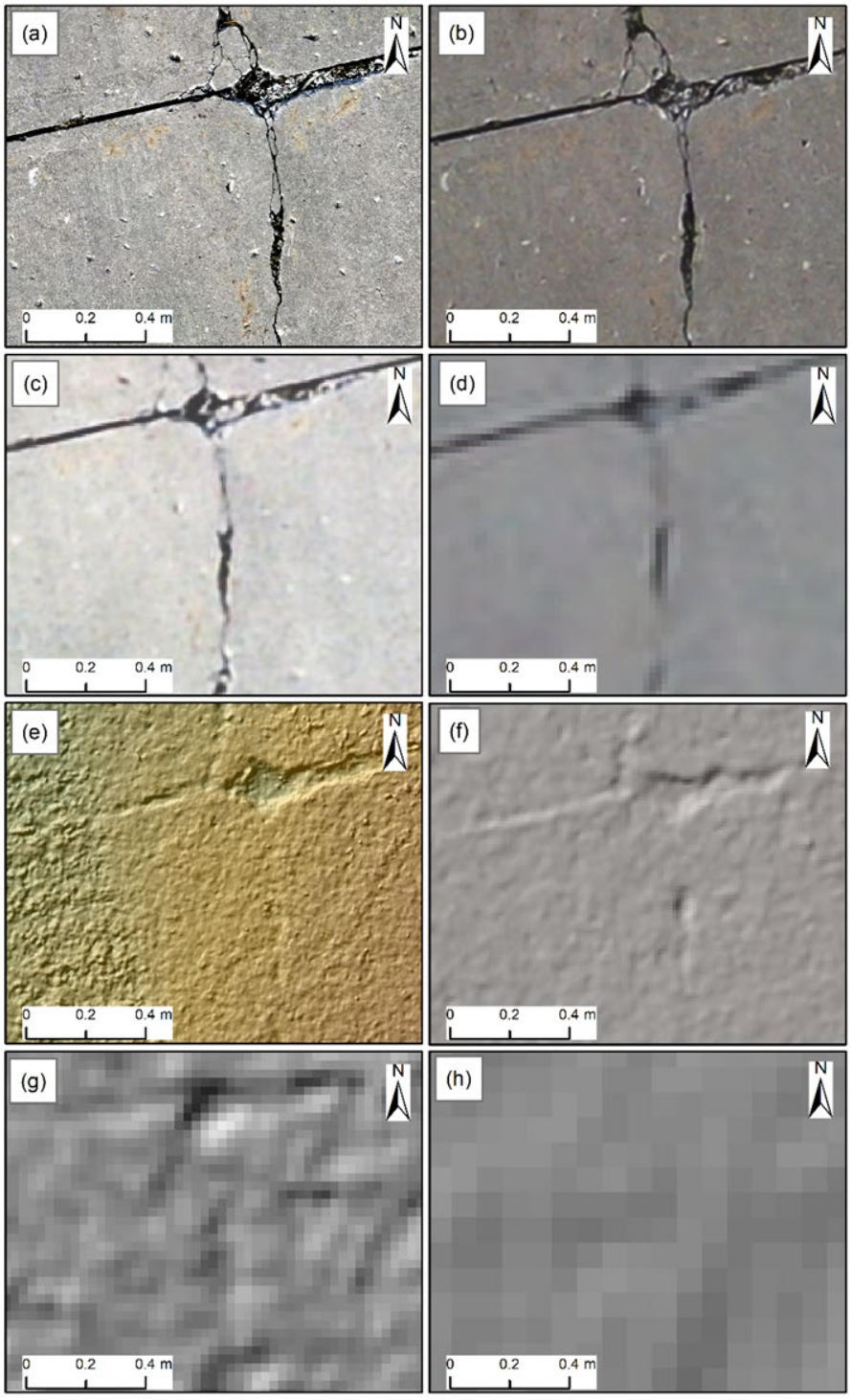

Figure 8. Longitudinal, Transverse, and Diagonal Cracks (M) and Durability Cracking (M) in (a) 0.8-mm/pix Orthophoto, (b) 2.5-mm/pix Orthophoto, (c) 7.3-mm/pix Orthophoto, (d) 21-mm/pix Orthophoto, (e) 3-mm/pix DEM, (f) 10-mm/pix DEM, (g) 29.1-mm/pix DEM, and (h) 84-mm/pix DEM

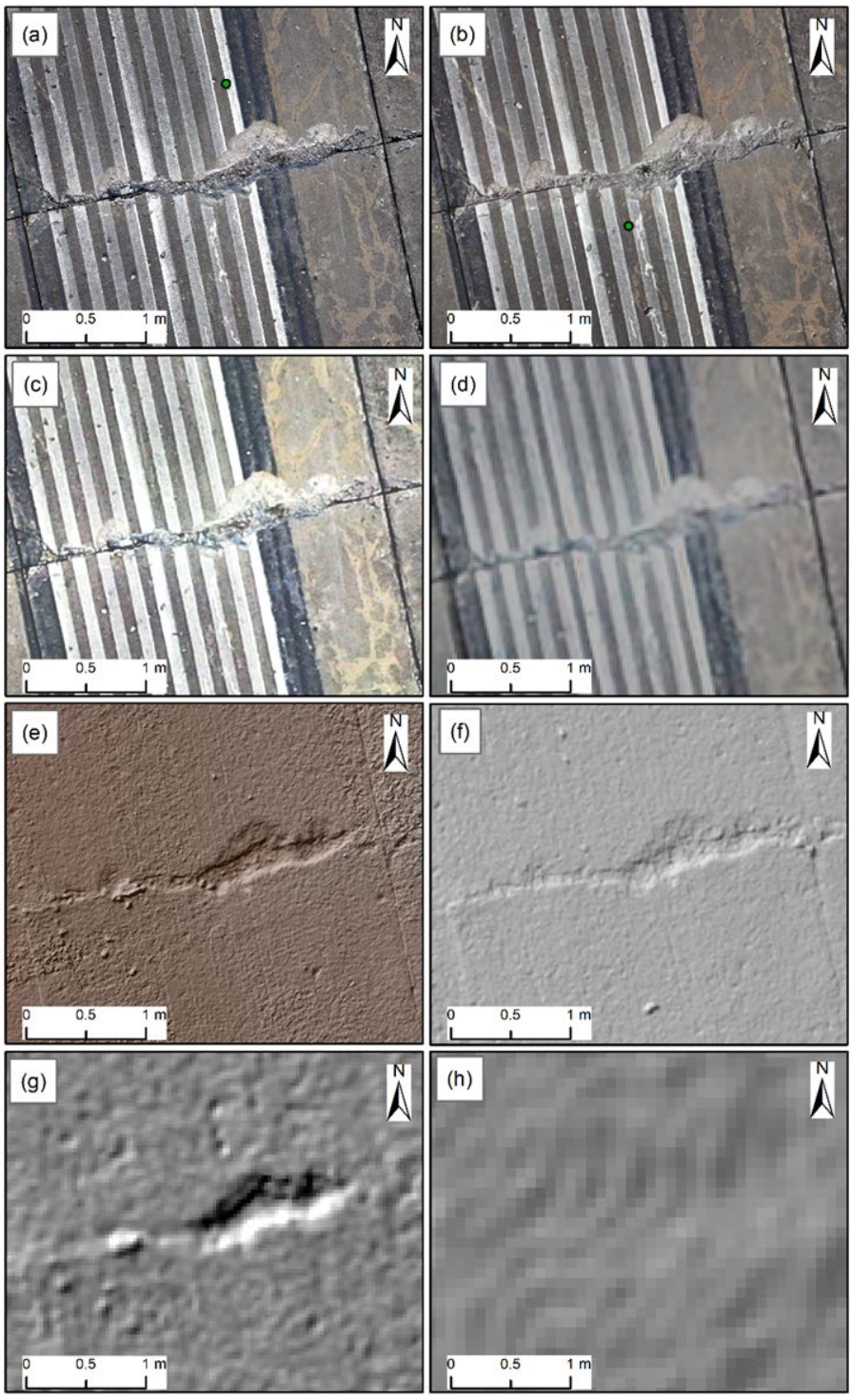

Figure 9. Durability Cracking (H) in (a) 0.8-mm/pix Orthophoto, (b) 2.5-mm/pix Orthophoto, (c) 7.3-mm/pix Orthophoto, (d) 21-mm/pix Orthophoto, (e) 3-mm/pix DEM, (f) 10-mm/pix DEM, (g) 29.1-mm/pix DEM, and (h) 84-mm/pix DEM

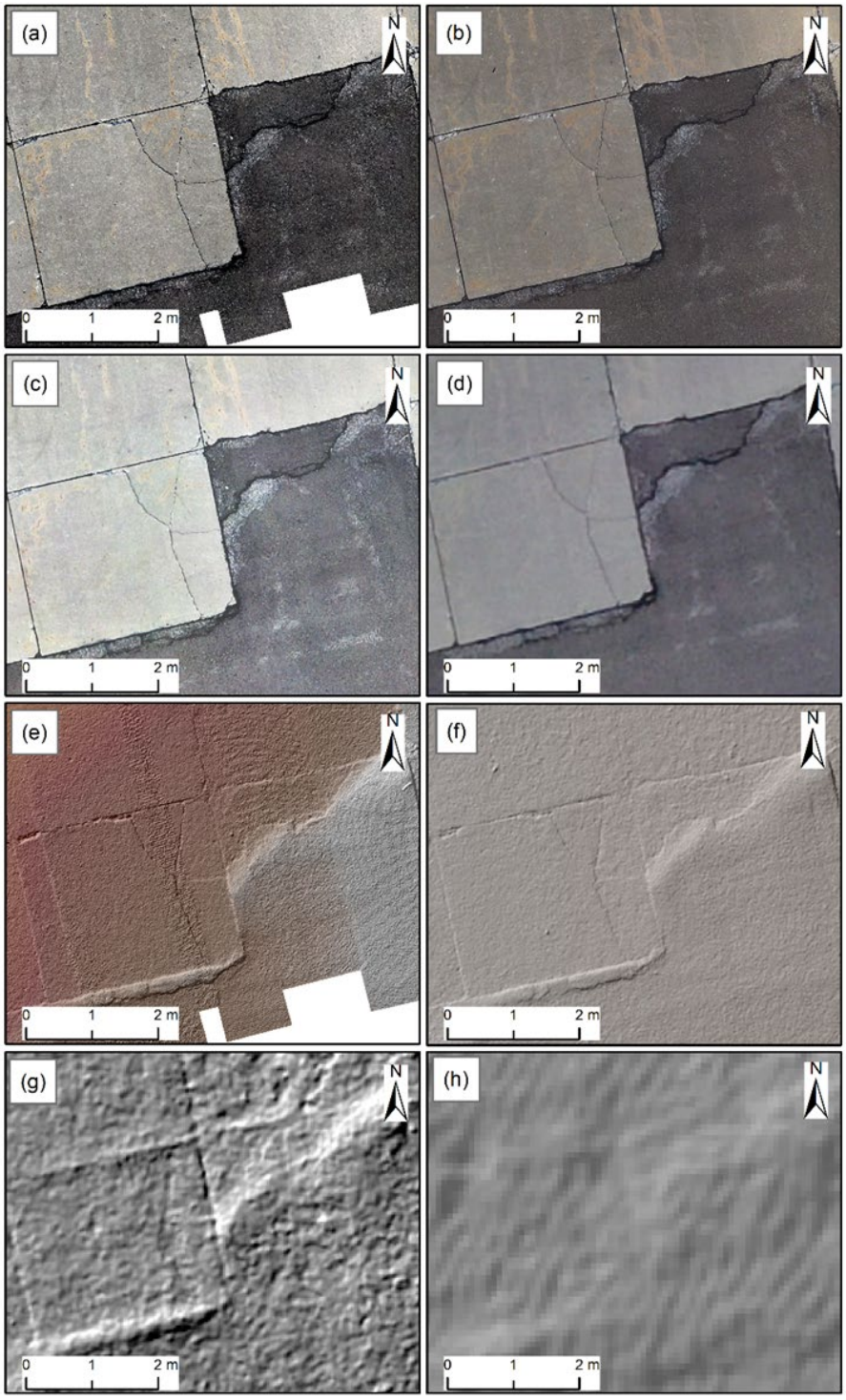

Figure 10. Shattered Slab (M), Large Patch (H), ASR (L) in (a) 0.8-mm/pix Orthophoto, (b) 2.5-mm/pix Orthophoto, (c) 7.3-mm/pix Orthophoto, (d) 21-mm/pix Orthophoto, (e) 3-mm/pix DEM, (f) 10-mm/pix DEM, (g) 29.1-mm/pix DEM, and (h) 84-mm/pix DEM

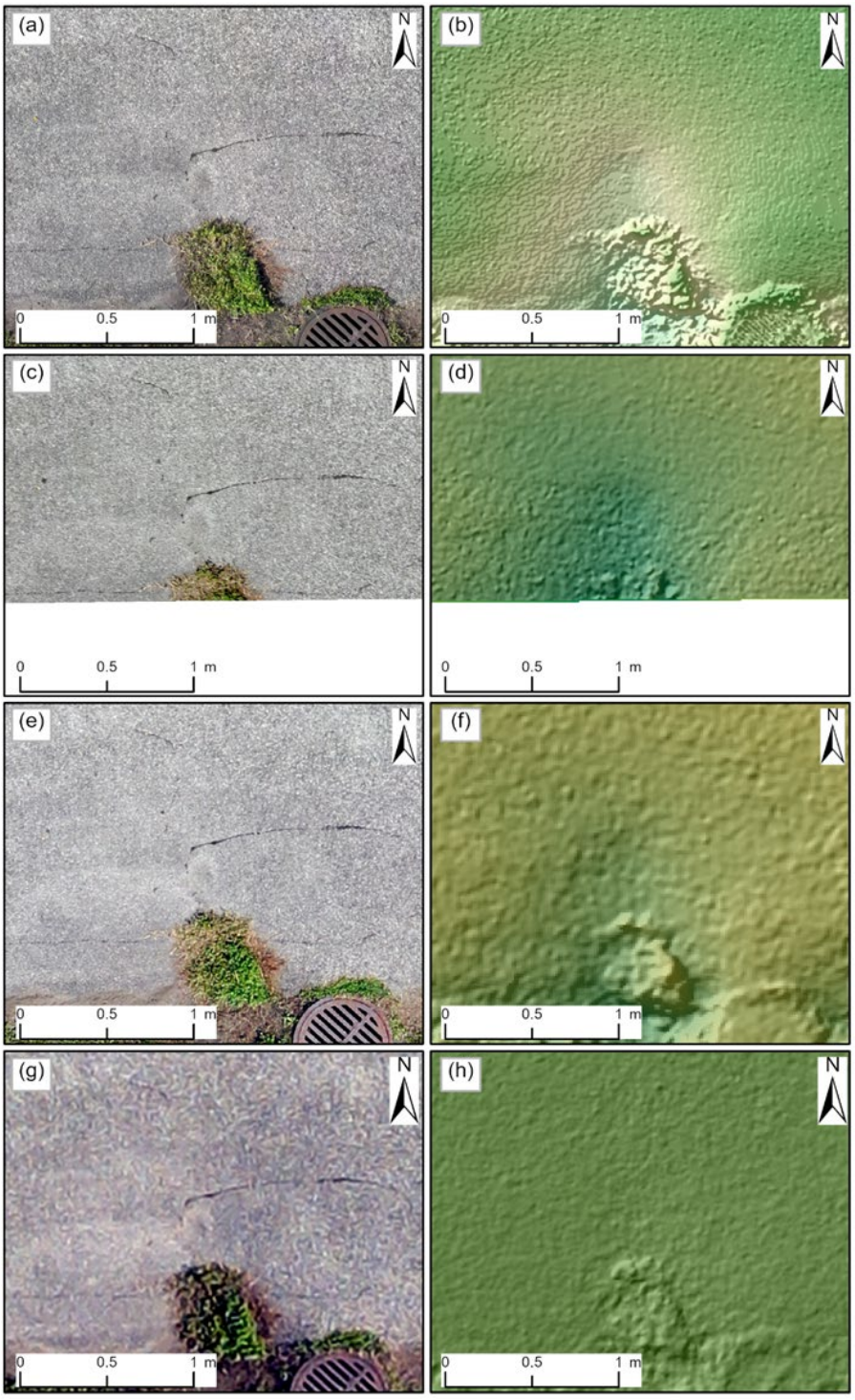

Figure 11. Depression in (a) 1.5-mm/pix Orthophoto, (b) 5.9-mm/pix DEM, (c) 2.2-mm/pix Orthophoto, (d) 8.9-mm/pix DEM, (e) 3.5-mm/pix Orthophoto, (f) 14-mm/pix DEM, (g) 4.1-mm/pix Orthophoto, and (h) 16.2-mm/pix DEM

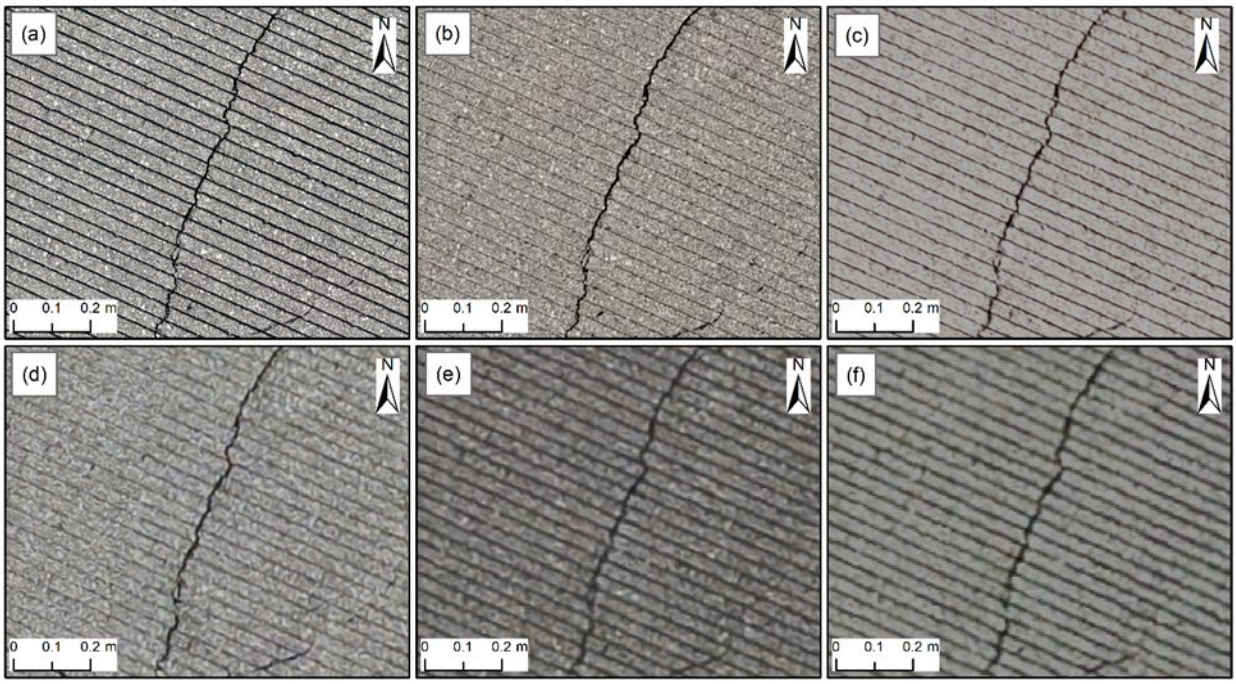

Figure 12. Unsealed Longitudinal and Transverse Cracks (L) and Weathering (L) on Asphalt Overlay Over Asphalt Concrete Pavement at TTF: (a) 0.8-mm/pix Orthophoto, (b) 1.5-mm/pix Orthophoto, (c) 2.3-mm/pix Orthophoto, (d) 2.5-mm/pix Orthophoto, (e) 4.9-mm/pix Orthophoto, and (f) 5.7-mm/pix Orthophoto

6.2 DIGITAL ELEVATION MODEL DATA

As discussed in section 5, DEMs are two-dimensional data products where each cell of the data represents the elevation value for an area. The DEM is produced during the structure-from-motion (SfM) and 3D processing in Agisoft Metashape®. This DEM is produced when using SfM software because it is a required intermediate step to produce an orthophoto. This study demonstrated that pavement distresses with elevation change could be detected and measured using the DEM data. The suspected locations of faulting of PCC pavement, and depression and shoving of AC pavement, could be confirmed using the high-resolution DEMs of at least 6.0 mm/pix or better. In addition, the presence of the faulting on the PCC pavement showed a significant elevation difference that could be used to confirm the suspected location of faulting in a slab.

Figure 13 shows the usefulness of high-resolution DEM data in detecting and verifying a change in elevation that helps indicate the presence of a distress. The two slabs where faulting exists at their edges show height differences of approximately 10 mm (1 cm or 0.01 m), as shown in parts (a) and (b); where no faulting exists, a rapid elevation “drop” is not present, as shown in (c) and (d). With this high-resolution DEM data, it is also possible to “drape” the orthophoto imagery on top of the DEM in a 3D view using GIS software to display how elevation changes of just a few centimeters can be captured through the sUAS surveys.

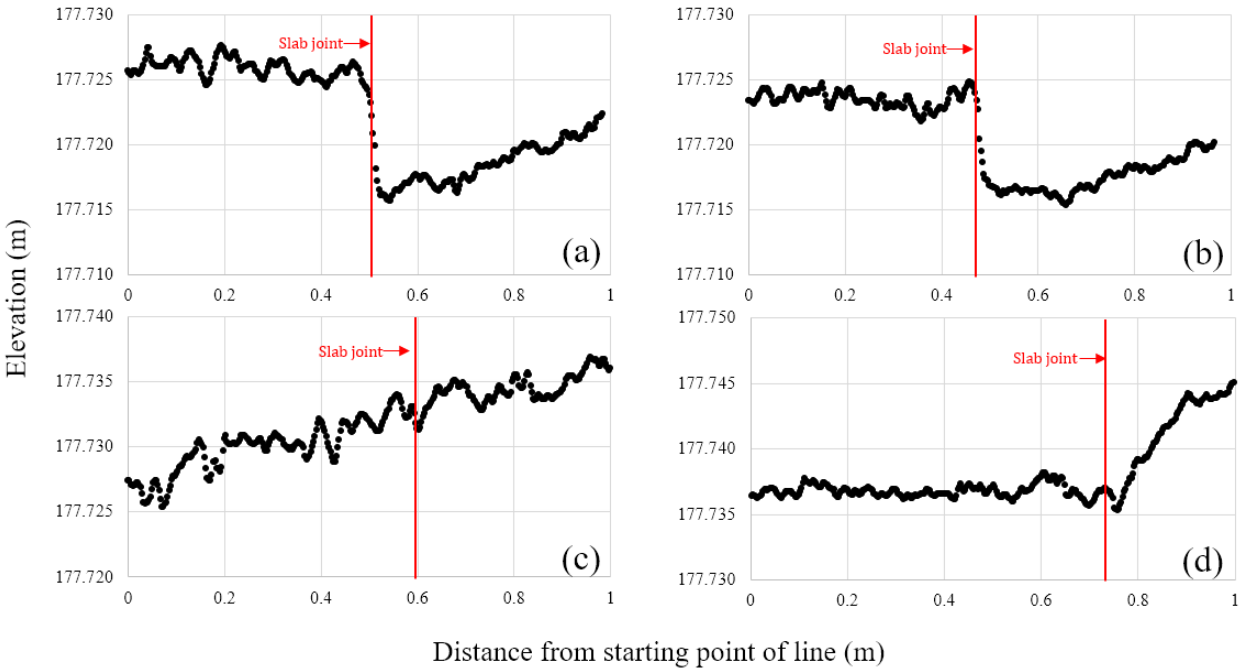

Figure 13. Medium-Severity Faulting Detection in 3-mm/pix DEM; (a, b) Slab Joint with the Faulting Shows a 1-cm Elevation Drop and (c, d) Slab Joint Without Faulting with no Drop

Figure 14 shows an oblique 3D view of a 2.5-mm resolution orthophoto, draped on top of a 10-mm resolution DEM collected in May 2021 at ONZ. A 5-cm difference exists between the highest point of the asphalt patch and the surrounding edges of the concrete slabs, which can be visualized in GIS software such as ArcGIS Pro that was used to create this image.

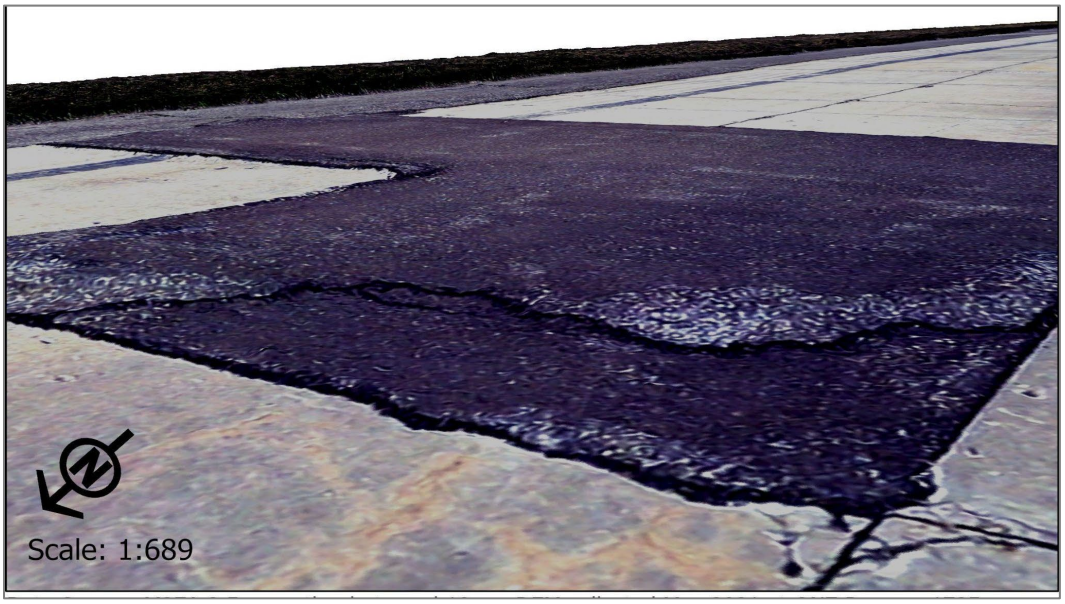

Figure 14. Draping an sUAS-derived Orthophoto on Top of a DEM to Show Elevation Differences for an Area of Patching on an Airport Runway

6.3 THERMAL DATA

The analysis of stereo thermal data has been more limited than the RGB orthophoto and DEM analyses thus far in the study (see discussion in section 3 on thermal sensors), but it has shown promising performance in detecting L&T cracks of AC pavement and LTD cracks and spalling of PCC pavement (Figures 15 and 16). The L&T cracks of AC pavement underneath the pavement markings, and those recently overlaid with a layer of concrete, showed significantly different heat signatures than other sections of the AC pavement. It is recommended to conduct further investigation of the value of thermal data for distress detection, potentially in a dedicated task or study.

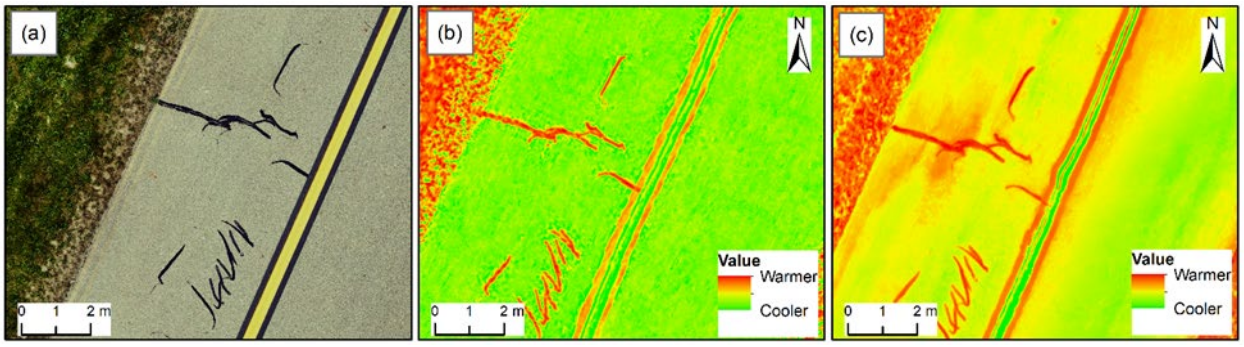

Figure 15. Sealed L&T Cracks on AC Pavement in Taxiway A Sample Unit 23 at TTF: (a) 1.5-mm/pix Orthophoto, (b) 31-mm/pix Stereo Thermal, and (c) 14-mm/pix Stereo Thermal

6.4 DIFFERENT DATA TYPES AND RESOLUTIONS USEFUL FOR DIFFERENT DISTRESSES

Based on the usefulness of the above-mentioned data types, a summary of different data resolutions and types that worked well for different distress identification and rating by an image analyst are provided in Tables 2 and 3.

Based on Table 2, Table 3, and visual analysis of sUAS data, the following resolutions for sUAS output products are recommended:

- Any sUAS system producing an orthophoto with resolutions smaller than (better than) 5 mm/pix can detect and rate at least some distresses. This resolution excludes the orthophoto generated from data collected using Quad Bayer optical RGB sensors interpolating 12-mp images to 48-mp outputs. Resolutions better than 2 mm/pix produce the best data for identifying and rating the largest number of distresses. The 1.5-mm/pix orthophoto and 6.0-mm/pix DEM combination was found to be the best resolution in terms of data collection and processing time and visual details.

- Any sUAS system producing a DEM and stereo-thermal orthophoto with resolutions better than 20 mm/pix and 30 mm/pix, respectively, is likely to be useful for distress detection and rating for at least some distress types.

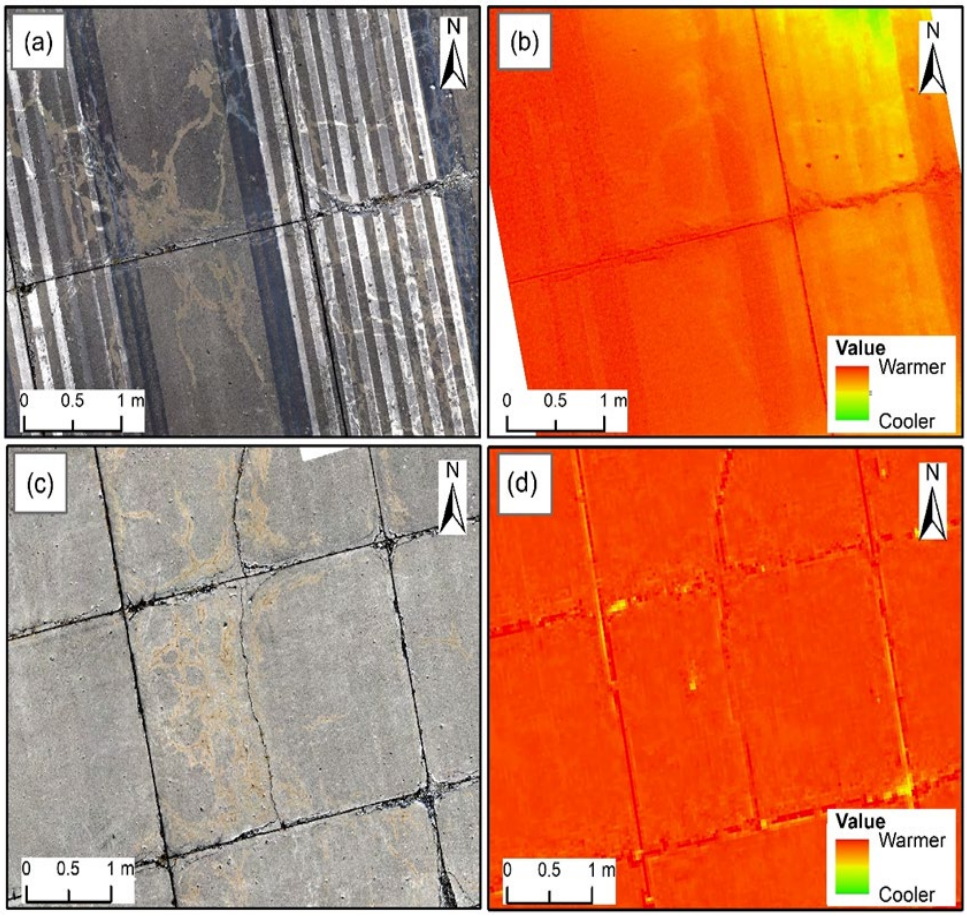

Figure 16. Longitudinal, Transverse, and Diagonal Cracks and Diagonal Cracks on PCC Pavement in Runway 17/35, Section 20 at ONZ: (a) 1.5-mm/pix Orthophoto of Sample Unit 5, (b) 8-mm/pix Stereo Thermal of Sample Unit 5, (c) 1.5-mm/pix Orthophoto of Sample Unit 23, and (d) 31-mm/pix Stereo Thermal of Sample Unit 23

Table 2. Distresses and Resolutions for PCC

ASTM Distress	Severity	Minimum Resolution (mm/pix)		Airport(s) with Distress
		Orthophoto	DEM	
Blowup (61)				Data not available
Corner break (62)	L	2.5	ND	ONZ, BNW, PRO, MTO, WWD
	M, H	21	ND	
LTD cracks (63)	L	7.3	ND	ONZ, BNW, PRO, MTO, WWD
	M	21	ND	
	H*	21	NA	
Durability cracking (64)	L	7.3	ND	ONZ
	M	21	10	
	H	21	29.1	
Joint seal damage (65)	L	ND	ND	BNW, PRO, MTO, WWD
	M	2.5	ND	BNW, PRO, WWD
	H	7.3	6	ONZ, BNW, PRO
Small patching (66)	L	3.3	ND	BNW, PRO, WWD
	M	4.5	6	BNW, PRO, WWD
	H*	4.5	6	PRO
Large patching (67)	L	21	ND	ONZ, BNW, PRO, WWD
	M, H	21	29	ONZ, WWD
Popouts (68)	NA	3.3	6	BNW
Pumping (69)	NA			Data not available
Scaling (70)	L			Data not available
	M, H*	21	10	ONZ
Settlement or faulting (71)	L	ND	ND	ONZ, PRO, WWD
	M, H*	ND	3	ONZ, PRO, WWD
Shattered slab (72)	L	ND	ND	
	M, H	21	10	ONZ, PRO
Shrinkage cracks (73)	NA**	2.5	ND	MTO, WWD
Joints spalling (74)	L**	2.5	ND	MTO, BNW, PRO, WWD
	M**, H	2.5	6	
Corner spalling (75)	L**, M**	3.3	ND	MTO, BNW, PRO, WWD
	H	3.3	10	PRO
ASR (76)	L**	7.3	ND	ONZ, BNW, PRO, WWD
	M**, H	7.3	6	ONZ, BNW, PRO, WWD

*Based on the detection of lower severity
**Detection not always possible or misidentified as other distresses
NA = Not applicable, ND = Not detected,
L = Low severity, M = Medium severity, H = High severity

Table 3. Distresses and Resolutions for AC

ASTM Distress	Severity	Minimum Resolution (mm/pix)		Distresses Available
		Orthophoto	DEM	
Alligator cracking (41)	L	3.5	5.9	WWD
	M, H			Data not available
Block cracking (43)	L	7.3	9.2	MTO, WWD
	M, H	7.3	19.6	
Corrugation (44)	NA			Data not available
Depression (45)	L	ND	ND	WWD
	M	ND	6	TTF, WWD
	H	4.1	16	WWD
Jet blast erosion (46)	NA			Data not available
Joint reflection cracking (47)	NA			Data not available
L&T cracking (48)	L	7.3	9.2	TTF, MTO, WWD
	M, H	7.3	19.6	
Oil spillage (49)				Data not available
Patching (50)				Data not available
Polish aggregate (51)				Data not available
Raveling (52)	L, M, H*	1.5	ND	TTF, WWD
Rutting (53)	NA			Data not available
Shoving (54)	L	ND	5.9	WWD
	M	2.5	10	MTO, WWD
Slippage cracking (55)				Data not available
Swell (56)	L, M	ND	ND	TTF, WWD
	H			Data not available
Weathering (57)	L, M, H	ND	ND	TTF, MTO, WWD

*Based on the detection of lower severity
**Detection not always possible or misidentified as other distresses
NA = Not applicable, ND = Not detected,
L = Low severity, M = Medium severity, H = High severity

6.5 DISTRESS CATEGORIES

Based on the sUAS data visual analysis at all six airports, the distress detection and rating could be divided into three categories. The summary of the categories is summarized in Table 4 followed by their details below.

6.5.1 Detectable

These distresses do not need any additional information apart from the sUAS data to be detected. Their location could be identified by visually observing the sUAS data, mainly RGB optical orthophotos. Alligator cracking (LMH), L&T cracking (LMH), block cracking (LMH), patching (LMH), and raveling (M) are detectable AC pavement distresses in this category. However,

detection of raveling (M) is not always possible. The low-severity alligator cracking present at study sites was detected; thus, it is safe to assume that medium- and high-severity alligator cracking will be detected. Corner break (LMH), LTD cracks (LMH), durability cracking (LMH), joint seal damage (MH), small patching (LMH), large patching (LMH), popouts, scaling (MH), shattered slab (LMH), shrinkage cracks, joints spalling (MH), corner spalling (MH), and ASR (MH) of PCC pavement are also in this category. Detection of shrinkage cracks is not always possible with the tested technologies; they can often be sub-millimeter in size. New digital cameras with 100-mp or greater resolution that are becoming available could help with detection and rating of very small distresses in the future. Joint spalling and corner spalling can also be identified as ASR, and ASR can be identified as spalling.

6.5.2 Detectable with Previous PCI Data

Some distresses require previous PCI data to be available to identify and rate them accurately. The distresses associated with vertical height differences are the most common in this category. Depression and shoving of AC pavement and faulting of PCC pavement show pavement surface movement vertically. An area with shoving goes up, depression goes down, and faulting exhibits elevation difference with adjacent slabs. The DEM outputs were found to be valuable for these distress detections, including when visualized with the aid of a 35 percent transparent hillshade displayed on top of the DEM in GIS software, such as ESRI ArcMap and ArcGIS Pro. This should be possible in other GIS software, such as QGIS, but this software was not tested during this study. It is not feasible to run a stack profile algorithm of ArcGIS Pro in every part of the sample units to identify the elevation-related distresses using DEM. However, if an area of the pavement is suspected of having elevation-related distresses or if a previous PCI report noted such distress, the possibility of that distress can be confirmed by running the stack profile algorithm on DEM. There are often visual similarities in low- and medium-severity joint spalling, corner spalling, and ASR. In some cases, it is hard to distinguish them by physically looking at the pavement, and additional laboratory testing is required for accurate identification. Previous PCI inspection results can assist in accurately identifying these distresses. Low- and medium-severity raveling detection is challenging as it does not produce easily viewable differences in even the highest resolution orthophotos and DEMs our team has produced so far. Historical PCI inspection data can assist in confirming the locations as well.

6.5.3 Undetectable in this Study

In this study, the distresses in this category were seldom identified consistently or could not be identified using even the highest resolution sUAS data. Low-severity joint seal damage cannot be identified by visually looking at it in the field or on an sUAS image. According to the *Concrete Surfaced Airfields Paver™ Distress Identification Manual*, the presence of low-severity joint seal damage can be confirmed by inserting a knife blade between the sealer and joint face without resistance (U.S. Army Corps of Engineers, 2009). Thus, these distresses are categorized as undetectable via sUAS. In some cases, low-severity ASR, swell, and all-severity weathering do not show any traits present in the sUAS products tested in this study.

Table 4. Types of Distresses

Type	Portland Cement Concrete Pavement Distresses	Asphalt Concrete Pavement Distresses
Detectable	Corner break (LMH), LTD cracks (LMH), Durability cracking (LMH), Joint seal damage (MH), Small patching (LMH), Large patching (LMH), Popouts, Scaling (MH), Shattered slab (LMH), Shrinkage cracks, Joints spalling (MH), Corner spalling (MH), ASR (MH)	Alligator cracking (LMH), L&T cracking (LMH), Block cracking (LMH), Patching (LMH), Raveling (H)
Detectable with previous PCI data	Faulting (LMH), Joints spalling (LM), Corner spalling (LM), ASR (LM)	Raveling (MH), Depression (LMH), Shoving (LMH)
Undetectable	Joint seal damage (L), ASR (L)	Swell (LM), Weathering (LMH)

7. CONCLUSIONS

Small unmanned aircraft system (sUAS) data were successfully collected from six airports in Michigan, Illinois, Iowa, and New Jersey. Different data types were processed and analyzed for their usefulness in airfield pavement distress detection and rating. Available airfield distresses were assessed for their presence using visual interpretation in GIS software with several different resolutions of RGB optical orthophoto and DEM data. A set of potentially detectable distresses was also studied using stereo-thermal data.

Analysis showed that visual and thermal data could be used to identify many airport Portland cement concrete (PCC) and asphalt concrete (AC) distress types. High-resolution (below 5 mm/pix) red, green, and blue (RGB) orthophoto effectively identifies many distresses, with lower-resolution data sets useful for identifying a limited number of distresses. The Digital Elevation Models (DEMs) derived using RGB optical data were mainly useful in confirming the suspected location of the pavement distresses with elevation differences, such as faulting, shoving, depression, and medium- and high-severity crack-based distresses. The best outputs for identifying and rating the most distresses were 1.5-mm/pix orthophotos and 6.0-mm/pix DEMs derived via photogrammetry from sUAS-collected images with 45.7-mp resolution.

Thermal data were shown to be useful for identifying certain distresses and foreign object damage as they exhibit a different thermal profile compared to intact concrete or asphalt pavement. High-accuracy (< 10 cm) positioning data for ground control points (GCPs) are valuable for accurately orienting orthophotos, creating high-quality DEM outputs, and for accurately aligning output products and traditional PCI survey data for distress evaluation. This also allows for the layering/stacking of various data sets and improves the ease with which one can compare data sets between years and different data collectors and will better track distress changes over time.

This study also discusses minimum crew requirements for efficient data collection, with three people recommended for the pilot, dedicated observer, and logistics assistant roles. The number of

GCPs required for accurate data collection was discussed, with a GCP approximately every 100 m along runways to create reliably high-quality data. sUAS platforms and sensors demonstrated in this study were reviewed to describe their effective deployment to meet different study requirements. Ensuring that flight control software and sUAS firmware are not changed immediately before data collection is helpful to successful data collection. In addition, scheduling sUAS deployment during weather conditions with no precipitation and acceptable winds was also recommended.

With sufficient sensor resolution, tested sUASs, use of GCPs, a properly staffed field crew, reasonable computing power, well-aligned output products, and PCI data, this study has shown that orthophotos and DEMs derived from photogrammetry are able to detect 13 of 14 PCC pavement distresses and 8 AC pavement distresses that were present at these airports. Most severity levels for these distresses could also be evaluated. These lessons learned will be used next to create input for a draft technical brief to be considered by the FAA for potential future publication.

8. REFERENCES

Airsight. (2020a). *Airfield pavement inspections using drones*. https://www.airsight.de/projects/item/airfield-pavement-inspections-using-drones/

Airsight. (2020b). *Runway pavement inspections using airsight drone*. https://www.airsight.de/projects/item/runway-pavement-inspections-using-airsight-drone/

Banks, E., Cook, S. J., Fredrick, G., Gill, S., Gray, J. S., Larue, T., Milton, J. L., Tootle, A., Wheeler, P., Snyder, P. R., & Waller, Z. (2018). *Successful Approaches for the Use of Unmanned Aerial System by Surface Transportation Agencies*. https://domesticscan.org/download/4364/

Brooks, C., Dobson, R., Banach, D., Oommen, T., Zhang, K., Mukherjee, A., Havens, T., Ahlborn, T., Escobar-Wolf, R., Bhat, C., Zhao, S., Lyu, Q., & Marion, N. (2018). *Implementation of Unmanned aerial vehicles (UAVs) for assessment of transportation infrastructure-Phase II*. https://rosap.ntl.bts.gov/view/dot/36994

Dobson, R. J., Colling, T., Brooks, C., Roussi, C., Watkins, M. K., & Dean, D. (2014). Collecting Decision Support System Data through Remote Sensing of Unpaved Roads. *Transportation Research Record: Journal of the Transportation Research Board*, *2433*(1), 108–115. https://doi.org/10.3141/2433-12

ESRI. (2021). *Hillshade function—ArcGIS Pro|Documentation*. https://pro.arcgis.com/en/pro-app/2.7/help/analysis/raster-functions/hillshade-function.htm

FHWA. (2018). *Use of Unmanned Aerial Systems (UAS) by State DOTs*. https://rosap.ntl.bts.gov/view/dot/43679

GSMArena. (2019). *Quad Bayer Sensors: What they are and what they are not*. https://www.gsmarena.com/quad_bayer_sensors_explained-news-37459.php

Hubbard, S., Pak, A., Gu, Y., & Jin, Y. (2017). UAS to Support Airport Safety and Operations: Opportunities and Challenges. *Journal of Unmanned Vehicle Systems*. https://doi.org/10.1139/juvs-2016-0020

Humpe, A. (2020). Bridge Inspection with an Off-the-Shelf 360° Camera Drone. *Drones*, *4*(4), 67. https://doi.org/10.3390/drones4040067

National Academies of Sciences, Engineering, and M. (2020). Airports and Unmanned Aircraft Systems, Volume 3: Potential Use of UAS by Airport Operators. In *Airports and Unmanned Aircraft Systems, Volume 3: Potential Use of UAS by Airport Operators* (Vol. 3). National Academies of Sciences, Engineering, and Medicine. https://doi.org/10.17226/25607

Seo, J., Duque, L., & Wacker, J. (2018). Drone-enabled bridge inspection methodology and application. *Automation in Construction*, *94*, 112–126. https://doi.org/10.1016/j.autcon.2018.06.006

Sourav, M. A. A., Ceylan, H., Brooks, C., Peshkin, D., Kim, S., Dobson, R., Cook, C., Brouillette, O., & Iowa State University. Department of Civil, C. and E. E. (2022). *Small Unmanned Aircraft System for Pavement Inspection: Task 4—Execute the Field Demonstration Plan and Analyze the Collected Data*. https://doi.org/10.21949/1524511

Sourav, M. A. A., Ceylan, H., Kim, S., Brooks, C., Peshkin, D., Dobson, R., Brynick, M., & DiPilato, M. (2022). Small Uncrewed Aircraft Systems-Based Orthophoto and Digital Elevation Model Creation and Accuracy Evaluation for Airfield Portland Cement Concrete Pavement Distress Detection and Rating. *International Conference on Transportation and Development 2022*, 168–180. https://doi.org/10.1061/9780784484371.016

Sourav, M. A. A., Mahedi, M., Ceylan, H., Kim, S., Brooks, C., Peshkin, D., Dobson, R., & Brynick, M. (2022). Evaluation of Small Uncrewed Aircraft Systems Data in Airfield Pavement Crack Detection and Rating. *Transportation Research Record: Journal of the Transportation Research Board*, 036119812211010. https://doi.org/10.1177/03611981221101030

U.S. Army Corps of Engineers. (2009). *Concrete Surfaced Airfields Paver™ Distress Identification Manual*. https://www.faa.gov/documentLibrary/media/Advisory_Circular/Concrete-Surfaced-Airfields-Distress-Manual.pdf